ARGONNE NATIONAL LABORATORY, ARGONNE, ILLINOIS

Operated under Contract W-31-109-Eng-38 for the
U. S. DEPARTMENT OF ENERGY

NOTICE

Proc. of the 6th Int'l. Conf. on Atomic Collisions in Solids,
[illegible], 1979, Hamilton, Canada

LASER FLUORESCENCE SPECTROSCOPY OF SPUTTERED URANIUM ATOMS*

R. B. WRIGHT, M. J. PELLIN, D. M. GRUEN and C. E. YOUNG
Chemistry Division, Argonne National Laboratory, Argonne, IL 60439

ABSTRACT

Laser induced fluorescence (LIF) spectroscopy was used to study the sputtering of 99.8% U^{238} metal foil when bombarded by normally incident 500-3000 eV Ne^+, Ar^+, Kr^+ and O_2^+. A three-level atom model of the LIF processes is developed to interpret the observed fluorescent emission from the sputtered species. The model shows that close attention must be paid to the conditions under which the experiment is carried out as well as to the details of the collision cascade theory of sputtering. Rigorous analysis shows that when properly applied, LIF can be used to investigate the predictions of sputtering theory as regards energy distributions of sputtered particles and for the determination of sputtering yields. The possibility that thermal emission may occur during sputtering can also be tested using the proposed model. It is shown that the velocity distribution (either the number density or flux density distribution, depending upon the experimental conditions) of the sputtered particles can be determined using the LIF technique and that this information can be used to obtain a description of

*Work performed under the auspices of the U.S. Department of Energy.

the basic sputtering mechanisms. These matters are discussed using the U-atom fluorescence measurements as a basis.

Both the v-parallel (the exciting laser beam is parallel to target surface) and the v-perpendicular (the laser beam is perpendicular to the target surface) number density velocity distributions were measured using the LIF Doppler shifted absorption frequencies of the sputtered ground state U(I) atoms. The results are compared with the collision cascade sputtering theory using the LIF model presented here. The relative sputtering yields for various incident ions on uranium were also measured for the first time using the LIF technique.

A surprisingly high fraction of the sputtered uranium atoms were found to occupy the low lying metastable energy levels of U(I). The population of the sputtered metastable atoms were found approximately to obey a Boltzmann distribution with an effective temperature of 920 ± 100°K.

I. Introduction

With the advent of continuously tuneable lasers the application of laser induced fluorescence (LIF) to the investigation of the spectroscopy of atoms and molecules and their dynamics has greatly increased in recent years (1,2). The LIF technique permits the determination of the number density and, via the Doppler shift, the velocity of the particle in a given atomic or molecular state. Basically the light of a given frequency, or frequency bandwidth, is used to induce a transition from a given lower to an upper level,

and the spontaneous emission from the upper level to an arbitrary lower level is measured. From the fluorescent intensity the population of the laser light-coupled levels can be deduced (3-6). If the laser light frequency is varied to access those atoms or molecules whose transition frequencies have been Doppler shifted due to a non-zero velocity component in the direction of the laser beam then their velocity distribution may also be determined by investigation of the fluorescent intensity as a function laser frequency (7-12).

Recently the LIF technique has been applied to the study of ion beam-surface interactions, specifically to the study of the sputtering process (LIFSP) (13-20). The utilization of LIF to study the sputtering process enables, in principle, the determination of absolute sputtering yields and also the measurement of the velocity (energy) distribution of not only the sputtered neutral atoms, but also the sputtered secondary ions and the sputtered excited neutrals and secondary ions.

The LIF techniques also shows promise as an in-situ diagnostic for controlled fusion devices as a means to determine the densities of neutral and, possibly, ionic particles, especially the plasma impurities (14,15,18,19).

In this paper we present LIF measurements of uranium metal when bombarded by Kr^+, Ar^+, Ne^+ and O_2^+ ions of 0.5-3 keV energy. Relative sputtering yields have been determined for normally incident ions and the number density velocity distributions have been measured. The secondary photon emission spectrum was also observed and will be briefly discussed.

II. Experimental Procedure

A schematic diagram of the experimental arrangement is shown in Figure 1. It consists of a continuous wave (CW) dye laser for production of the excitation light, a target assembly and vacuum system, an ion gun for irradiation of the target, and an optical detection system.

The excitation source was a continuous wave dye laser (Coherent Radiation #CR-595) pumped by an argon-ion laser (Coherent Radiation #CR-12) operating on the 514nm transition. Rhodamine 6G (2×10^{-3}M) was the dye used to excite all the resonance transitions utilized here. The dye laser itself was operated with one 5mm etalon and a three element Lyot filter. This produced a spectral output which included three longitudinal laser modes. Each mode has a time averaged frequency width of $\sim$ 10 MHz. The spacing between the modes was 0.3GHz giving a velocity resolution in the unsaturated regime of $\approx 2 \times 10^{4}$ cm/sec. The laser power was determined with a pyroelectric radiometer (Laser Precision #RK3440). The instrument was accurate to at least 5%.

The vacuum system was constructed out of 304SS using internal welds and Conflat flange copper gasketed seals. The main pumping was done with a 3-inch oil (Santovac-5) diffusion pump with a L-N_2 baffle. One 25l/s and one 8 l/s ion pump were also used. After bakeout to 200°C, base pressures of 2×10^{-9} torr were achieved. The main chamber (see Figures 2 and 3) in which the target, optical baffles and laser beam entrance and exit windows, as well as the sputter ion gun were located was a 2.75" 6-way UHV cross from Huntington Mechanical Laboratories, Inc. The UHV vacuum windows for the laser entrance and exit windows were type 7056 glass; the window used for the observation of the LIF emission or the secondary photon emission was either type 7056 glass or LiF. The

optical baffles for the laser beam entrance and exit were used to reduce the amount of scattered laser light which could enter the detection system and were made from chemically blackened OFHC copper fittings consisting of alternating internally threaded cylinders and flat disks with beveled (60°) 3.8 mm holes in their center (5 of each were used in each arm). These fittings were then slid inside of a 304SS tube with Conflat flanges on each end which was in turn fastened to the 6-way cross. The target was mounted on the end of a UHV linear translation feedthrough for the $v_{||}$ measurements as shown in Figure 2. The translator was used to position the target with respect to the laser beam; the ion gun could be refocussed to maintain the same ion beam spot size. For the $v_{\perp}$ measurements, see Figure 3, the target was mounted on a metal platform which had a hole drilled down its center which permitted the passage of the laser beam through a 1 mm hole in the center of the target. The laser beam was thus normal to the target surface, exciting the LIF emission in front of the target from the atoms which were sputtered by the normally incident ion beam. Since the laser beam was dumped directly into the ion gun, a great deal of scattered laser radiation was produced. In this sampling geometry we were forced because of this circumstance to induce a transition at one frequency, say from the ground state to an excited state, but then in order to circumvent scattered radiation to observe fluorescence emitted at a different frequency by decay to an intermediate metastable excited state. In both the $v_{||}$ and $v_{\perp}$ configurations the

fluorescent emission was observed at right angles to the ion beam and the target surface normal.

A Varian sputter ion gun was used as the source of energetic ions in these studies. When operating the ion gun the target chamber oil diffusion pump was throttled, the ion pumps shut off and the chamber backfilled to an equilibrium value of 8×10^{-5} torr, via a UHV leak valve, with the desired sputtering gas. The incident ion energy could be varied between 500 eV and 3 keV. The total ion current was usually maintained at 20 μamp. The FWHM of the ion beam was approximately 6mm. The target was biased at +90 volts to suppress secondary electron emission. Prior to recording the LIF data, the target was extensively sputter-cleaned, but the target's surface composition was not independently monitored.

The optical detection system was composed of two plano-convex Optical Crown glass lenses from Melles Griot, 50 mm dia. with 100 mm and 300 mm (nearest the spectrometer) focal lengths which were used to collect the optical emission from the experiment. The collection solid angle was 1.56×10^{-2}. The collected light was analyzed with a McPherson Model 218 single monochromator which had a 1200 groove/mm grating blazed at 5000 Å. The dispersed light was detected with a cooled (-20°C) RCA C31034A-02 PMT operating at 1500 volts (dark count was 5 cps). The PMT output was amplified and counted used an Ortec photon counting system.

The uranium target was a piece of depleted U^{238} (99.8%) foil

0.6 mm thick. The foil was degreased in solvent, and then etched with nitric and hydrofluoric acid before placing it in the target chamber. No abrasive polishing was done.

Figure 4 shows the various neutral uranium energy levels which were studied in this paper (21).

III. Results and Discussion

Prior to presenting our experimental results we will describe the LIF technique and how it may be used to investigate the sputtering process. We will use as a model for the LIF process one which involves three atomic energy levels, one state labeled 1, energy ν_1, is assumed to have a population density of n_1^o atoms $\cdot$ cm^{-3} and an upper level labeled 2, energy ν_2, to which level 1 can be excited by resonance absorption of the laser photons of frequency ν(Hz). Level 2 is assumed to have an initial population density of zero at t = 0, ie. n_2 (t = 0) = 0. Level 2 may decay by spontaneous emission and stimulated emission to level 1, and by spontaneous emission only to a third level, labeled 3, energy ν_3 the value of which can be $\nu_2 > \nu_3 > \nu_1$ or $\nu_2 > \nu_1 > \nu_3$. Level three is assumed to be stable (infinite lifetime) and to have a zero or non-zero population density, n_3^o, at t = 0. We will also assume that the spectral width of the laser beam is broader than the natural line width of the atomic transition (refer to references 4,19,22 and 23 for a discussion of this point). When this three level system is exposed to a laser beam of

intensity $I(\nu)$ having an energy flux density of joules $\cdot$ cm^{-2} $\cdot$ sec^{-1} $\cdot$ Hz^{-1}, or a power density in watts $\cdot$ cm^{-2} $\cdot$ Hz^{-1}, at the resonant frequency ν, the time rate of change of the population density in the three levels can be written as:

$$\frac{dn_1}{dt} = -n_1 B_{12}(I/c) + n_2 B_{21}(I/c) + n_2 A_{21} \qquad (1)$$

$$\frac{dn_2}{dt} = -n_2\left[A_{21} + A_{23} + B_{21}(I/c)\right] + n_1 B_{12}(I/c) \qquad (2)$$

$$\frac{dn_3}{dt} = n_2 A_{23} \qquad (3)$$

In equations 1-3, c is the speed of light in cm $\cdot$ sec^{-1}, A_{21} and A_{23} are the spontaneous emission transition rates from level 2 to level 1 and level 3 respectively in sec^{-1}, B_{12} and B_{21} are the Einstein coefficients for absorption and stimulated emission respectively between levels 1 and 2 with units cm $\cdot$ g^{-1}. We may reexpress equations 1-3 by using the relationships between the Einstein coefficients: $g_1 B_{12} = g_2 B_{21}$, $B_{21} = A_{21}/(8\pi h\nu^3/c^3)$ where g_1 and g_2 are the degeneracies of levels 1 and 2 respectively, and by defining a quantity:

$$\begin{aligned} S &= I(\nu)/(8\pi h\nu^3/c^2) \\ &= 8.51 \times 10^{-18}\ (P/D^2) \cdot (\lambda^5/\Delta\lambda) \\ &= 6.87 \times 10^{52}\ (P/D^2)/(\nu^3\Delta\nu) \end{aligned} \qquad (4)$$

where P is the laser power in watts, for a beam diameter D in cm and of wavelength λ and linewidth $\Delta\lambda$ in nm or of frequency ν and linewidth $\Delta\nu$ in Hz^{-1}. Equations 1-3 may be rewritten in the form:

$$\frac{dn_1}{dt} = -n_1 A_{21}(g_2/g_1)S + n_2 A_{21}(1 + S) \tag{5}$$

$$\frac{dn_2}{dt} = -n_2(A_{23} + A_{21}(1 + S)) + n_1 A_{21}(g_2/g_1)S \tag{6}$$

$$\frac{dn_3}{dt} = n_2 A_{23} \tag{7}$$

These coupled differential equations may now be solved using Laplace transforms and the relationships $n_1^o = n_1(t) + n_2(t) + n_3(t)$ to arrive at the expressions for $n_1(t)$, $n_2(t)$ and $n_3(t)$. We are actually only interested in the population of level 2 since it is the radiative decay of this level which gives rise to the LIF emission. The time dependence of the population of level 2 is then given by:

$$n_2(t) = \frac{n_1^o A_{21}(g_2/g_1)S}{[a^2 - b]^{\frac{1}{2}}} \cdot \exp(-at) \cdot \sinh\left[(a^2 - b)^{\frac{1}{2}}t\right] \tag{8}$$

where:

$$a = \tfrac{1}{2}\left[A_{21}\left[1 + S\left(\frac{g_1 + g_2}{g_1}\right)\right] + A_{23}\right] \tag{9}$$

$$b = A_{21}A_{23}(g_2/g_1)S \tag{10}$$

If $A_{23} = 0$ equation 8 reduces to the two level (levels 1 and 2 only) case where $n_2(t)$ is given by:

$$n_2(t) = \frac{n_1^o}{\left[1 + (g_1/g_2)\left(1 + \frac{1}{S}\right)\right]} \cdot \left\{1 - \exp\left[-A_{21}\left[1 + S\left(\frac{g_1 + g_2}{g_1}\right)\right]t\right]\right\} \tag{11}$$

Equation 8 for the population density in level 2 for the three level system has rather different saturation conditions, ie. when S is large, than does equation 11 for $n_2(t)$ of a two level system. When S is very large for the three level system

$$n_2^{sat}(t) = n_1^o\left(\frac{g_2}{g_1 + g_2}\right)\exp\left[-\left(\frac{g_2}{g_1 + g_2}\right)A_{23}t\right] \tag{12}$$

whereas for the two level system equation 11 reduces to:

$$n_2^{sat}(t) = n_1^o\left(\frac{g_2}{g_1 + g_2}\right) \tag{13}$$

Therefore, when S >> 1 (ie. I(ν) is very large) for the three level system the population in level 2 decreases the longer the atom remains in the laser beam (the atoms are pumped over into

[illegible] and [illegible] there), but the population in level 2 for the [illegible] system [illegible] with time. [illegible] the [illegible] in both cases.

When S = 1 the population of level 2 for the three level [illegible]:

$$n_2(t) = \frac{n_1^o \sigma_{12}(\nu_2 - \nu_1) S}{(A_{21} + A_{23})} \left[1 - \exp\left[-(A_{21} + A_{23})t\right]\right] \qquad (14)$$

[illegible] when S = 1 for the two level case:

$$n_2(t) = n_1^o \sigma_{12}(\nu_2 - \nu_1) S \left[1 - \exp(-A_{21} t)\right] \qquad (15)$$

From equations 14 and 15 it is seen that [illegible] in both cases the population in level 2 is proportional to S, i.e. to the laser intensity. [illegible] the three level system (equation 3) at any value of S approaches $n_2(\infty) = 0$ [illegible] not all of the atoms which have been excited from level 1 to level 2 will end up in level 3. This is quite different from the two level case (equation 11) where the population in level 2 as $t \to \infty$ approaches:

$$n_2(\infty) = \frac{n_1^o}{\left[1 + \frac{g_1}{g_2}\left(1 + \frac{1}{S}\right)\right]} \qquad (16)$$

The time variable t given in the above equations can be defined in several ways depending upon the experimental situation. Time

t = 0 can be defined to coincide with the laser being pulsed "on" or when the atom enters the laser beam in the case of a CW laser. Thus t = 0 can be defined to be when the laser is turned "on", or when the atom exits the laser beam. We have assumed in the above and in what follows that the system employed to detect the fluorescent photons collects light only from the region defined by the exciting laser beam.

We can now define a photon yield function Y(v,t) to represent the number of fluorescent photons due to the decay of level 2 to level 1 produced by an atom in level 1 entering the exciting laser beam with a velocity v and undergoing excitation and de-excitation for a time t as:

$$Y(v,t) = \frac{1}{n_1^o(v)\,\Delta V} \cdot A_{21}\,\Delta V \int_0^t n_2(t,v)\,dt \qquad (17)$$

where the yield and the number densities n_1^o and n_2 are expressed as functions of the atomic velocity, v, a point which will be used later in our discussion of the Doppler shift. ΔV in equation 17 is the effective volume of the exciting laser beam determined by the laser beam diameter and the collection optics of the detection system. Integrating equation 17 by substituting from

[illegible]

$$[illegible] \qquad (18)$$

with a and b as previously defined in equations [illegible] and [illegible]. The number of fluorescent photons which are produced per second for those atoms moving with a velocity v is then given by:

$$N(v,t) = \frac{n_1^0(v) \cdot V \cdot Y(v,t)}{t} \qquad (19)$$

At saturation (S [illegible] 1) combining equations 12, 17 and 19 yields N(v,t) [illegible]

$$N(v,t) = \frac{n_1^0(v)\ V(A_{21}/A_{23})}{t} \cdot \left[1 - \exp\left[-\left(\frac{g_2}{g_1 + g_2}\right)A_{23}t\right]\right] \qquad (20)$$

If the repetition rate of a pulsed laser is less than the transit time of the atom through the laser beam t can be defined as the duration of the laser pulse. When a CW laser is being used then t can be defined as the transit time of an atom with velocity v through the laser beam

of diameter D(8). In this case t = D/vcosθ where θ is defined with respect to the normal to the laser beam axis. The collection optics, expecially when using a monochromotor with finite slits, may also define a D dimension. If the pulse duration of the laser is smaller than the spontaneous emission rate A_{23} or if, in the CW laser case $A_{23}D/v\cos\theta \ll 1$ due to a small D or large v, then the exponential term in equation 20 can be expanded. The result including terms up to second order is:

$$N(v) = n_1^o(v)\Delta V A_{21}\left(\frac{g_2}{g_1 + g_2}\right) \qquad (21)$$

Under the experimental conditions of S >> 1 (ie. large I(.)), and either a small laser pulse duration, or small D or high v for the CW laser case, the number of fluorescent photons emitted per second for atoms moving with a velocity v is proportional to the number density of the atoms. It is apparent then from equation 21 that by using the LIF technique the number density velocity distribution for sputtered atoms can be determined if these experimental conditions are met and if the three level model is a valid one for the fluorescent process. In the case when S >> 1 but $A_{23}D/v\cos\theta \gg 1$ then N(v,t) from equations 20 is:

$$N(v) = n_1^o(v)\ V(A_{21}/A_{23} \cdot \left(\frac{v}{D}\right) \cdot \cos\theta \qquad (22)$$

In this case $N(v) \propto n_1^o(v) \cdot v$ which is the flux density velocity distribution. Obviously one should be fully aware of the experimental conditions under which the data are obtained. The distinction between the number and the flux density velocity distributions and their dependence on the experimental conditions appears not to have fully appreciated in prior publications on this topic.

Using the same method as that discussed above, when $S << 1$ (ie. low laser intensity) then for the three level case $N(v,t)$ is found to be:

$$N(v,t) = \frac{n_1^o(v) \cdot \Delta V \cdot A_{21}^2 (g_2/g_1) S}{(A_{21} + A_{23})} \cdot \left\{ 1 + \left[(A_{21} + A_{23}) t \right]^{-1} \cdot \right.$$

$$\left. \cdot \left[\exp\left[-(A_{21} + A_{23}) t \right] \right] \right\} \qquad (23)$$

As before, if the pulse duration is short $(A_{21} + A_{23})t << 1$, or if $(A_{21} + A_{23})D/v\cos\theta << 1$ as for the CW laser case, then equation (23) reduces to:

$$N(v,t) = n_1^o(v) \cdot \Delta V \cdot A_{21}^2 (g_2/g_1) S(t/2) \qquad (24)$$

which for the case of a CW laser further reduces to $N(v,t) \propto n_1^o(v)/v$. When $(A_{21} + A_{23})t >> 1$, or if $(A_{21} + A_{23})D/v\cos\theta >> 1$ then equation 23 becomes:

$$N(v) = \frac{n_1^o(v) \cdot \Delta V \cdot A_{21}^2 (g_2/g_1) S}{(A_{21} + A_{23})} \qquad (25)$$

which in this case indicates that $N(v) \propto n_1^o(v)$.

In order to calculate the number of sputtered atoms with velocity v which enter the laser beam we will assume a flux density velocity distribution, $\#\cdot cm^{-2}\cdot sec^{-1}\cdot (\text{unit velocity})^{-1}$, displayed by neutral atoms sputtered by a collision cascade process. Thompson (24) and Sigmund (25,26) have presented models for such a flux density velocity distribution which has the following analytic form (27,28) for atoms sputtered with $(v + dv, \theta + d\theta, \phi + d\phi)$.

$$\Phi(v,\theta) \sin\theta dv d\theta d\phi = \frac{C(n) v^3 \cos\theta \sin\theta dv d\theta d\phi}{(v^2 + v_b^2)^{n+1}} \qquad (26)$$

where θ is the polar angle defined with respect to the target surface normal and ϕ is the azimuthal angle. v_b is the velocity corresponding to the surface binding energy E_b, ie. $v_b = (2E_b/M_2)^{\frac{1}{2}}$, which arises due to the assumed planar potential barrier that the cascade atom must overcome in order to escape the target surface. n is a variable which is generally $1 \leq n \leq 2$. Equation 18 is thought to be valid when the incident ion beam is perpendicular to the target surface. The constant C(n) is given by:

$$C(n) = \frac{(6.242 \times 10^{12} J\cdot S)}{\pi \int_o^{v_m} \frac{v^3 dv}{(v^2 + v_b^2)^{n+1}}} \qquad (27)$$

where J is the incident ion beam current density in $\mu amp \cdot cm^{-2}$, S is the neutral atom sputtering yield for incident ions impinging normal to the target surface, and v_m is the maximum energy which can be transferred to a target atom by a collision with an incident ion of energy E_1 and mass M_1 as given by:

$$v_m = \left[\frac{4M_1M_2}{(M_1 + M_2)^2} \cdot \frac{2E_1}{M_2}\right]^{\frac{1}{2}} \qquad (28)$$

The integral appearing in equation 19 has previously been evaluated for various values of n (28). It can be shown that the flux density velocity distribution given by equation 26 increases as v^3/v_b^{2n} when $v << v_b$, reaches a maximum at

$$v_{max} = \left[3/(2n-1)\right]^{\frac{1}{2}} v_b \qquad (29)$$

and decreases as $v^{-(2n-1)}$ when $v >> v_b$. The sputtered neutral atom number density velocity distribution n(v), # · cm^{-3} · (unit velocity)$^{-1}$ is related to the flux density velocity distribution by (11):

$$n(v,0) = \frac{1}{v} \cdot \Phi(v,0) \qquad (30)$$

Equation 30 gives the number density velocity distribution which should be used in equation 19 ($n(v,0) \equiv n_1^o(v)$) to calculate the number of fluorescent photons · sec^{-1}, N(v,t), produced in an LIF experiment assuming a collision cascade mechanism for the sputtering process. If the total sputtering yield is to be determined by the LIF method, then the integral over all velocities of equation 19 via equations 18 and 26-30 is required so that N(v,t) is proportional to the sputtering yield, S. Obviously from equations 19 and 26-30 the LIF technique may be used to determine the number density velocity distribution of the sputtered neutral atoms and thereby the number density energy distribution since $n(v)/v \propto n(E)$. The corresponding flux density velocity and flux density energy distribution can also be determined since $vn(v) = \Phi(v)$ and $n(v) \propto \Phi(E)$.

When photoelectric detection using photon counting techniques with a detection efficiency of ε is used to determine the number

of LIF produced photons · sec^{-1} then the number of counts · sec^{-1} measured would be

$$Q = N(v) \cdot \varepsilon \cdot \frac{\Omega}{4\pi} \tag{31}$$

where Ω is the solid angle of acceptance of the detection equipment.

As discussed in the experimental section one can measure the sputtered neutral atom number density velocity distribution by decomposing the general velocity vector v of the sputtered atom into $v_{\parallel}$ and $v_{\perp}$ components defined with respect to the target surface. By measureing the Doppler shift of an atom with a non-zero velocity component in the direction of the exciting laser beam, one can, by sweeping the laser frequency through a frequency range about the non-shifted (zero velocity) resonant transition frequency, determine the number density of atoms which possess a given velocity and thereby the number density velocity distribution as discussed above. In an attempt to calculate the $v_{\parallel}$ Doppler profile determined in the present series of experiments we will assume a simple model in which the target is planar (one dimensional) lying along the x-axis parallel to the laser beam, which is also assumed to be one dimensional. The sputtered atoms are emitted with a cosθ distribution (see equation 26), θ defined with respect to the normal to the x-axis, ie., the axis. The number density velocity distribution is that given by equations 26 and 30; the sin $\theta d\phi$ term which arises due to solid angle considerations is

not included in this two dimensional model. Therefore,

$$n(v,\theta)dvd\theta = \frac{v^2 \cos\theta dvd\theta}{(v^2 + v_b^2)^{n+1}} \tag{32}$$

With the definition that $v_{||}$ is parallel to the x-axis, and $v_{\perp}$ is parallel to the z-axis, then:

$$v = (v_{||}^2 + v_{\perp}^2)^{\frac{1}{2}} \tag{33}$$

$$\cos\theta = \frac{v_{\perp}}{(v_{\perp}^2 + v_{||}^2)^{\frac{1}{2}}} \tag{34}$$

$$vdvd\theta = dv_{\perp}dv_{||} \tag{35}$$

Using the Doppler shift relation for the $v_{||}$ component (ν_o is the non-shifted resonant transiton frequency and c the speed of light):

$$v_{||} = \frac{-c(\nu-\nu_o)}{\nu_o} \tag{36}$$

$$dv_{||} = \frac{-c}{\nu_o} d\nu \tag{37}$$

Equation 32 may then be rewritten as

$$n(v_{\perp},v_{||})dv_{\perp}dv_{||} = \frac{v_{\perp}dv_{\perp}dv_{||}}{(v_{\perp}^2 + v_{||}^2 + v_b^2)^{n+1}} \tag{38}$$

$$n(v_{\perp},\nu)dv_{\perp}d\nu = \frac{v_{\perp}dv_{\perp}d\nu}{\left[v_{\perp}^2 + (\frac{c}{\nu_o})^2(\nu-\nu_o)^2 + v_b^2)\right]^{n+1}} \tag{39}$$

We have defined $v_{||}$ and $v_{\perp}$ to be along the direction of the laser beam, corresponding to a red shift of the fluorescence.

Integrating over $dv_\perp$ from 0 to ∞ (actually it should be from 0 to $v_m - v_b$, but since $v_m >> v_b$ and since integrating to $v_\perp = \infty$ makes little difference we have used this upper limit) we arrive at the general result for $n \geq 0$:

$$D_{||}^{n}(\nu)d\nu \propto \frac{d\nu}{\left[(\nu-\nu_o)^2 + (\frac{\nu_o v_b}{c})^2\right]^n} \tag{40}$$

or,

$$D_{||}^{n}(v_{||})dv_{||} \propto \frac{dv_{||}}{\left[v_{||}^2 + v_b^2\right]^n} \tag{41}$$

The profile-width (full width at half maximum) of the Doppler profile given by equation 29 is calculated to be:

$$\Delta\nu_{||}(n) = 2\left[(2)^{1/n} - 1\right]^{1/2}\cdot\left[\frac{\nu_o v_b}{c}\right] \tag{42}$$

From equations 40-42 it can be seen that the shape and profile-width of the experimental $v_{||}$ Doppler profile may be used to determine n and v_b in equation 32. Certainly this model is oversimplied as in reality when one does the LIF experiment a finite area on the target is being sputtered, the laser beam has a finite length and diameter and is a finite distance from the target surface. However, the above model should still be crudely applicable if the laser beam passed near the target surface and if the ion beam spot size is large compared to the dimensions of the excitation volume sampled by the detection system.

Mindful of the constraints discussed in the preceding paragraph, the $v_\perp$ Doppler profile would be that given by equation 32

integrated over cos $\theta d\theta$ and then making the substitution $v_\perp = v = \pm c(\nu-\nu_o)/\nu_o$, where the sign would have to be determined by the direction of the laser beam with respect to the $v_\perp$ direction. Therefore, the $v_\perp$ Doppler profile would be

$$D_\perp^n(\nu)d\nu \propto \frac{(\nu-\nu_o)^2 d\nu}{\left[(\nu-\nu_o)^2 + (\frac{\nu_o v_b^2}{c})\right]^{n+1}} \tag{43}$$

There may also arise a thermal component in the sputtered neutral atom yield which can occur either from a thermal spike (29,30) or simply due to an evaporation of the target surface in order for it to maintain chemical stoichiometry, as in the case of the alkali halides (13,20,31,32). The flux density velocity distribution for this sputtered component is generally given by the Maxwell-Boltzmann distribution for a gaseous effusion source:

$$\Phi_T(v)\ \sin\theta dv d\theta d\vartheta = \frac{2n}{\pi}\left(\frac{M_2}{2kT}\right)^2 \cdot v^3 \cdot \exp(-M_2 v^2/2kT) \cdot$$

$$\cdot \cos\theta \sin\theta dv d\theta d\phi \tag{44}$$

where n is the number of particles emitted per unit area per second, ie. $J \cdot S_T$ where J is the current density of the incident ion beam and S_T is the equivalent number of particles emitted per incident ion; k is Boltzmann's constant and T the effective temperature of the emission process in °K. The number density velocity distribution is found as before from equation 30. If we use the same simple model as outlined previously in equations 32-42 for the

Doppler profile of the $v_{||}$ velocity component we arrive at the equations:

$$D_T(\nu)d\nu = \left(\frac{c}{\nu_o}\right)\left(\frac{M_2}{2\pi kT}\right)^{\frac{1}{2}} \exp\left[-\left(\frac{M_2}{2kT}\right) \cdot \left[\frac{c(\nu-\nu_o)}{\nu_o}\right]^2\right] d\nu \qquad (45)$$

$$\Delta\nu_T = 2\left[2(\ln 2)\left(\frac{kT}{M_2}\right)\right]^{\frac{1}{2}} \cdot \left(\frac{\nu_o}{c}\right) \qquad (46)$$

for the $v_{||}$ Doppler profile (normalized to unity) and the profile-width respectively. It should be pointed out that the above result is independent of the power of v assumed in equation 44, but does of course depend on the assumed gaussian distribution.

In Figure 5 we show the experimentally determined $v_{||}$ Doppler profile for the ground state → 16900 cm^{-1} → ground state LIF spectrum for neutral U^{238} sputtered by 3 keV Kr^+. The experimental arrangement was that shown in Figures 1 and 2. The conditions under which the experiment was conducted would indicate that $(A_{21} + A_{23})D/\cos\theta \gg 1$ and $S \ll 1$ so that equation 25 would be the expression for the number of fluorescent photons per second emitted for a group of sputtered atoms moving with a velocity v. In Figure 2 we have converted the frequency scale (the exciting laser was tuned over a frequency range centered at 16900 cm^{-1}) into a velocity scale. Also shown in this figure are theoretical curves for n = 2 and n = 3/2 in equations 40-42. The value of $v_b = 2.092 \times 10^5$ cm/sec was used, corresponding to

a sublimation energy of E_b = 5.4 eV, for uranium metal. The best fit to the experimental data is given by $n = 1.75 \pm 0.10$ and $v_b = (2.09 \pm 0.20) \times 10^5$ cm/sec. The error limits are difficult to set as n and v_b are adjustable parameters, yet they do indeed correspond to values which have previously been determined for sputtered uranium. Using 9 keV Ar^+ to sputter uranium-238 metal the flux density velocity distribution was measured by Young, et al (33,34) using the nuclear fission-track density method for $1 \times 10^5 \leq v \leq 1.9 \times 10^6$ cm/sec. Their best fit to equation 18 was obtained when n = 1.78 and E_b = 5.35 eV. Weller and Tombrello (35), using the nuclear fission-track density method with a mechanical time-of-flight spectrum, measured the flux density energy distribution for 93% enriched U^{235} foil sputtered by 80 keV Ar^+ ions for $1 \leq E \leq 10^3$ eV. Their best fit to the flux density energy distribution analog [illegible] equation 26 gave [illegible].77 and E_b = 5.4 eV. These values of n are quite close to the value n = 1.7 which Williams (36) has arrived at from a more extensive treatment of the collision cascade sputtering process.

Figure 6 shows the experimental LIF $v_\perp$ Doppler profile for 3 keV Kr^+ bombardment of uranium. The experimental arrangement in this case is that shown in Figure 3. Due to the great amount of scattered laser light in this configuration we had to observe the LIF emission using the ground state → 16900 cm^{-1} → 3801 cm^{-1} pump and decay scheme. Therefore, the observed fluorescent emission

was at 763.17 nm which was well separated from the exciting laser wavelength of 591.54 nm, so that the stray laser light did not present [illegible]. In Figure 6 we also show two theoretical v_z Doppler profiles as calculated from equation 43. The peak position and the high velocity portion of the observed number density velocity distribution are best represented when n = 1.77 to 2 with $v_b = 2.092 \times 10^5$ cm/sec. The low velocity portion is also reproduced reasonably well with these parameters. The dashed line for the experimental data corresponds to our approximate velocity resolution of 2×10^4 cm/sec, so that we cannot with confidence determine the velocity distribution below this value.

v_z and v_- Doppler profiles were also measured using 3 keV Ar^+ and Ne^+ to bombard the uranium sample. Within our present experimental error we could not discern any noticeable difference in the Doppler [illegible] as compared to 3 keV Kr^+ incident ions as discussed above. From our measurements and from those of Young, et al (33,34) and Weller and Tombrello (35) the measured neutral ground state uranium atom flux density energy distribution is independent of the energy (for 3-80 keV) and mass (Ne, Ar, Kr) of the bombarding particle. This is expected from the collision cascade sputtering process as presently understood (24-26).

If we now integrate over the velocity number density velocity distribution over velocity, the result is proportional to the sputtering yield as was indicated in equations 26-30. In Table I we give the relative sputtering yields for neutral U^{238} atoms for 3 keV Kr^+, Ar^+ and Ne^+ incident ions as measured by integrating over the experimental LIF v number density velocity distributions. For comparison we also show in Table I the theoretical values as calculated by using the semi-empirical sputtering yield equation of Smith (37) and the theoretical treatment of Sigmund (25,26). The only other available experimental data for these three incident ions on uranium metal are those by Wehner (38) which are also shown in Table I. However, Wehner's values were taken at 500 eV in a plasma discharge which would imply a multitude of angles of incidence for the bombarding ions. Theoretically one would also not expect the relative sputtering yields to be the same at 500 eV as at 3 keV. Gregg and Tombrello (39) have recently measured the sputtering yield of U^{235} when bombarded with 13-120 keV protons, 40-120 keV He^+ and 40 and 80 keV Ar^+. They also found a discrepancy with the yields predicted using the Sigmund theory.

It is interesting to note that a uranium target bombarded with 3 keV O_2^+ in a background of 8×10^{-5} torr O_2 showed no LIF emission either from ground state or metastable state U^{238} atoms within the limitations of our signal-to-noise. We also tried to excite LIF emission from sputtered ground state U^+ using the U(II) groundstate → 18200 cm^{-1} → groundstate excitation-decay scheme but were unable to detect a signal either when O_2^+ was the bombarding ion or when either Kr^+, Ar^+ or Ne^+ was used. We would expect that the uranium surface would be highly oxidized when bombarding with an O_2^+ beam in a high pressure O_2 gas background. This should substantially increase the amount of neutral UO or UO_2 metal oxide sputtering relative to neutral U sputtering. From the SIMS data of Morgan and Werner (40) using 6 keV O_2^+ at various partial pressures of O_2 gas, at approximately 3×10^{-5} torr O_2 partial pressure with the O_2^+ beam the $O^+:O_2^+$ relative yields were approximately 4×10^{-3}:0.3:1 so it may not be surprising that U^+ was not observed with the LIF technique. With regard to the inert gas incident ions, the lack of detectable U^+ LIF emission may indicate that for relatively clean uranium metal the ion fraction is quite low. A drastic difference was also observed in the secondary photon emission spectrum when O_2^+ was used as the bombarding ion. With the inert gas incident ions emission from many U(I) and U(II) excited levels was observed over the 300-800 nm range whereas with the O_2^+ beam only a very broad, structureless continuum centered at 340 nm was observed. The origin of this emission is unknown, probably arising from the sputtered excited uranium oxide molecules.

A significant population of sputtered atoms in the three low lying metastable levels of U(I) was observed as shown in Figure 4. By tuning the laser to excite the metastable atoms at the wavelengths shown in Figure 4 the fluorescent radiation was measured either at the exciting wavelength or at a shorter wavelength due to emission from the excited level to the ground state. Using the $v_{||}$ experimental configuration (Figure 2) to determine the $v_{||}$ Doppler profile for each of the three low lying levels and then integrating these profiles we compared these integrals with that for the groundstate → 16900 cm^{-1} → groundstate $v_{||}$ Doppler profile integral discussed above. The results of these measurements with 3 keV Kr^+ incident ions is given in Table II. If these relative values are assumed to follow a Boltzmann distribution:

$$\frac{N_j}{N_i} = \frac{g_j}{g_i} \cdot \exp\left[-(E_j - E_i)/kT\right] \tag{47}$$

where in this case E_i is the energy of the ground state and the E_j's are the energies of the low lying excited states given in Table II as ΔE (cm^{-1}). The measured integrals of the $v_{||}$ profiles were corrected for the relevant branching ratios and for the relative efficiency of the detection system. The values do indeed appear to follow a Boltzmann distribution, but it must be noted that data exist for only three points and that there is a large uncertainty in the 3868 cm^{-1} value. The temperature as determined from

such a treatment yields a value of 920 ± 100°K. Whether or not the metastable population exhibits a true Boltzmann distribution remains [illegible] question. The fact remains that the low lying metastable levels of sputtered U(I) have an appreciable population. A similar population of the low lying levels of sputtered Fe(I) was also reported by Elbern (16) using the LIF technique. As noted earlier in this paper the $v_{||}$ Doppler profiles for the metastable levels are essentially describable by the collision cascade model. This would exclude a strictly thermal origin of the sputtered metastable atoms (refer to Figure 5 for an example of the theoretical thermal $v_{||}$ Doppler profile as compared to the collision cascade $v_{||}$ Doppler profile). It is also difficult to reconcile the temperature of the metastables with the secondary photon emission spectra observed in this study. By treating the observed secondary photon emission yields as being represented by a Boltzmann distribution with an "effective" temperature (41) corresponding to the excitation process, we determined a value of approximately 3800 ± 400°K. Further work is in progress to attempt to explain these observations especially by using different incident ions and at different incident energies as well as more refined measurements of the $v_{||}$ and $v_{\perp}$ Doppler profiles for the sputtered metastable atoms.

IV. Conclusions

We have been able to use the LIF technique to study many aspects of the sputtering of uranium metal by low energy ions.

Certainly with further refinements of the experimental methods a great deal of detailed information regarding the velocity (energy) distributions of not only the sputtered neutral atoms, but also of sputtered ions and excited atoms and ions should become available for many materials with careful and considered utilization of this method. Relative sputtering yields, and, with suitable calibration, absolute sputtering yield are also readily measured.

Table Captions

Table I. Relative sputtering yields for Kr^+, Ar^+ and Ne^+ at 3 keV, normally incident on uranium metal. The LIF values were determined in this work and are based only on the LIF of the sputtered ground state U^{238} atoms.

Table II. Relative population of the low lying energy levels of sputtered U^{238} as measured by the LIF technique (for 3 keV Kr^+ at normal incidence).

Table I.

Relative Sputtering Yields

Normally Incident Ion	LIF[a] (3 keV) (Neutral Atom)	Theory (3 keV) (Smith[b])	Theory (3 keV) (Sigmund[c])	Experiment (500 eV) (Wehner[d])
Kr^+	1	1	1	1
Ar^+	0.44	0.46	0.71	0.65
Ne^+	0.18	0.22	0.40	0.35

a) Determined from integration of LIF $v_{||}$ Doppler profile.

b) D. L. Smith, J. Nucl. Mater. 75, 20 (1978).

c) P. Sigmund, Phys. Rev. 184, 383 (1969).

d) G. K. Wehner, General Mills Report No. 2309, July (1962).

Table II.

Relative population of the low lying energy level of U^{238} as measured by the LIF technique (for 3 keV Kr^{+} at normal incidence):

State	$\Delta E(cm^{-1})$	g	Relative Population
$^5L_6^\circ$	0	13	1
$^5K_5^\circ$	620	11	0.21 ± 0.06
$^5L_7^\circ$	3801	15	$2.9 \times 10^{-3} \pm 1 \times 10^{-3}$
$^5H_3^\circ$	3868	7	$9.5 \times 10^{-4} \pm 1 \times 10^{-3}$

Temperature would correspond to 920 ± 100°K if a Boltzmann distribution is assumed.

Figure Captions

Figure 1. Diagram of the experimental arrangement used to study the sputtering process by the LIF technique (Refer to text for a detailed discussion).

Figure 2. Cross sectional view of the target chamber used to measure the v-parallel sputtered atom number density velocity distribution and the relative sputtering yields.

Figure 3. Cross sectional view of the target chamber used to measure the v-perpendicular sputtered atom number density velocity distribution.

Figure 4. Diagram of the energy levels of neutral U^{238} atoms which were investigated in this study. Energy level values are given in cm^{-1}; the wavelength of the transition is given by the bracketed values in nanometers.

Figure 5. Experimental data for the $v_{||}$ LIF Doppler profile for sputtered ground state neutral U^{238} atoms due to 3 keV Kr^{+} incident ions. The theoretical curves were calculated as discussed in the text.

Figure 6. Experimental data for the $v_{\perp}$ LIF Doppler profile, i.e. the number density velocity distribution, for sputtered groundstate neutral U^{238} atoms due to 3 keV Kr^{+} incident ions, The theoretical curves were calculated as discussed in the text.

References

(1) J. L. Kinsey, Ann. Rev. Phys. Chem. 28, 349 (1977).

(2) M. H. Nayfeh, American Scientist 67, 204 (1979).

(3) R. M. Measures, J. Appl. Phys. 39, 5232 (1968).

(4) P. Jacquinot, in: High Resolution Laser Spectroscopy, K. Shimoda, ed. (Springer-Verlag, New York, 1976) p. 52.

(5) D. E. Evans, in: Physics of Ionized Gases, B. Navinsek, ed. (J. Stefan Institute, Ljublijana, Yugoslavia, 1976) p. 641.

(6) P. Bogen and Y. T. Lie, Appl. Physics 16, 139 (1978).

(7) W. D. Phillips, D. Pritchard, Phys. Rev. Letters 18, 1254 (1974).

(8) I. V. Hertel, H. Hofmann and K. A. Rost, J. Physics E 8, 1023 (1977).

(9) T. D. Gaily, S. N. Rosner and R. A. Holt, Rev. Sci. Instrum. 47, 143 (1976).

(10) D. Hammer, E. Benes, P. Blum and W. Husinsky, Rev. Sci. Instrum. 47, 1178 (1976).

(11) J. L. Kinsey, J. Chem. Phys. 66, 2560 (1977).

(12) C. Y. She, W. M. Fairbanks, Jr. and K. W. Billman, Optics Letters 2, 30 (1978).

(13) W. Husinsky, R. Bruckmüller, P. Blum, F. Viehböck, D. Hammer and E. Benes, J. Appl. Phys. 48, 4734 (1977).

(14) A. Elbern, D. Rusbüldt and E. Hintz, Proc. Inter. Symp. Plasma Wall Interactions, Jülich (Pergamon Press, New York, 1977) p. 475.

(15) D. Rusbüldt, ibid., p. 483.

(16) A. Elbern, ibid., p. 489.

(17) M. J. Pellin, R. B. Wright, E. O. Rausch, C. E. Young and D. M. Gruen, Bull. Amer. Phys. Soc. 24 (1979) 497.

(18) A. Elbern, E. Hintz and B. Schweer, J. Nucl. Materials 76 & 77, 143 (1978).

(19) P. Bogen and E. Hintz, Comments Plasma Phys. Cont. Fusion 4, 115 (1978).

(20) W. Husinsky and R. Bruckmüller, Surf. Sci. 80, 637 (1979).

(21) J. Blaise and L. J. Radziemski, Jr., J. Opt. Soc. Am. 66, 644 (1976), and references therein.

(22) A. Yariv, Quantum Electronics, 2nd edition (John Wiley & Sons, New York, 1975) Chapter 8.

(23) J. Lipson, Thesis, University of California, San Diego, 1978 (General Atomic Company Report GA-A15029, June, 1978).

(24) M. W. Thompson, Phil. Mag. 18, 377 (1968).

(25) P. Sigmund, Phys. Rev. 184, 383 (1969).

(26) P. Sigmund, Rev. Roum. Phys. 17, 769, 897, 1005 (1972).

(27) J. Politiek and J. Kistemaker, Rad. Effects 2, 129 (1969).

(28) R. Wright and D. M. Gruen, J. Chem. Phys., to be published (1979).

(29) M. W. Thompson and R. S. Nelson, Phil Mag. 7, 2015 (1962).

(30) P. Sigmund, in: Ineleastic Ion-Surface Collisions, N.H. Tolk, J. C. Tully, W. Heiland and C. W. White, eds. (Academic Press, New York, 1977) p. 153.

(31) G. P. Können, J. Grosser, A. Haring, A. E. DeVries and J. Kistemaker, Rad. Effects 21, 171 (1974).

(32) M. Szymonski, H. Overeijnder and A. E. DeVries, Rad. Effects 36, 189 (1978).

(33) C. E. Young, P. M. Dehmer, R. B. Cohen, L. G. Pobo and S. Wexler, J. Chem. Phys. 64, 306 (1976).

(34) C. E. Young, R. B. Cohen, P. M. Dehmer, L. G. Pobo and S. Wexler, J. Chem. Phys. 65, 2562 (1976).

(35) R. A. Weller and T. A. Tombrello, Rad. Effects 37, 83 (1978).

(36) M. M. R. Williams, Phil. Mag. 34, 669 (1976).

(37) D. L. Smith, J. Nucl. Mater. 75, 20 (1978).

(38) G. K. Wehner, General Mills Report No. 2309, July (1962).

(39) R. Gregg and T. A. Tombrello, Rad. Effects 35, 243 (1978).

(40) A. E. Morgan and H. W. Werner, Surf. Sci. 65, 687 (1977).

(41) C. J. Good-Zamin, M. T. Shehata, D. B. Squires and R. Kelly, Rad. Effects 35, 139 (1978).

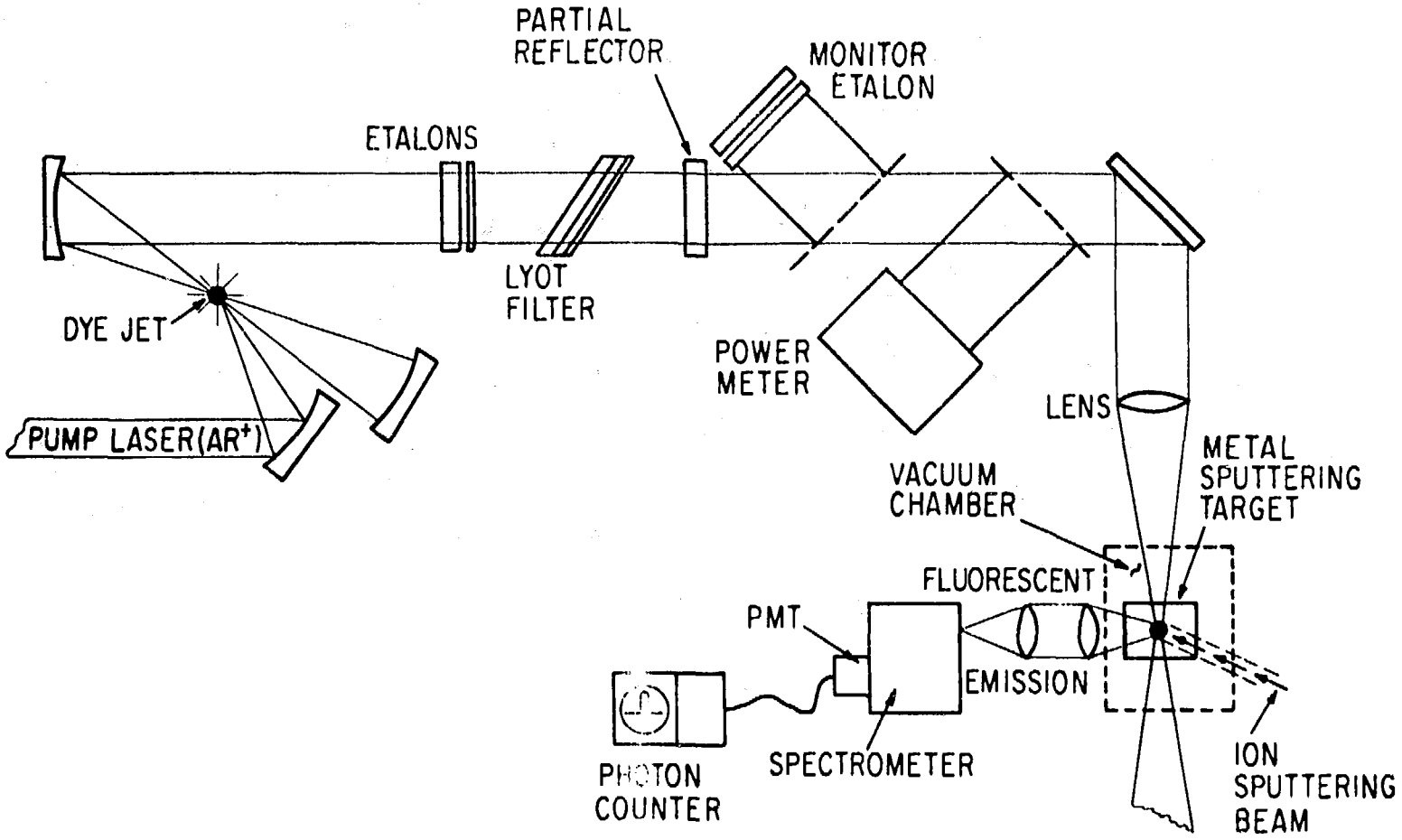
PARTIAL
REFLECTOR
MONITOR
ETALON
ETALONS
LYOT
FILTER
DYE JET
POWER
METER
LENS
PUMP LASER(AR+)
METAL
SPUTTERING
TARGET
VACUUM
CHAMBER
FLUORESCENT
PMT
EMISSION
PHOTON
COUNTER
SPECTROMETER
ION
SPUTTERING
BEAM

Fig.1

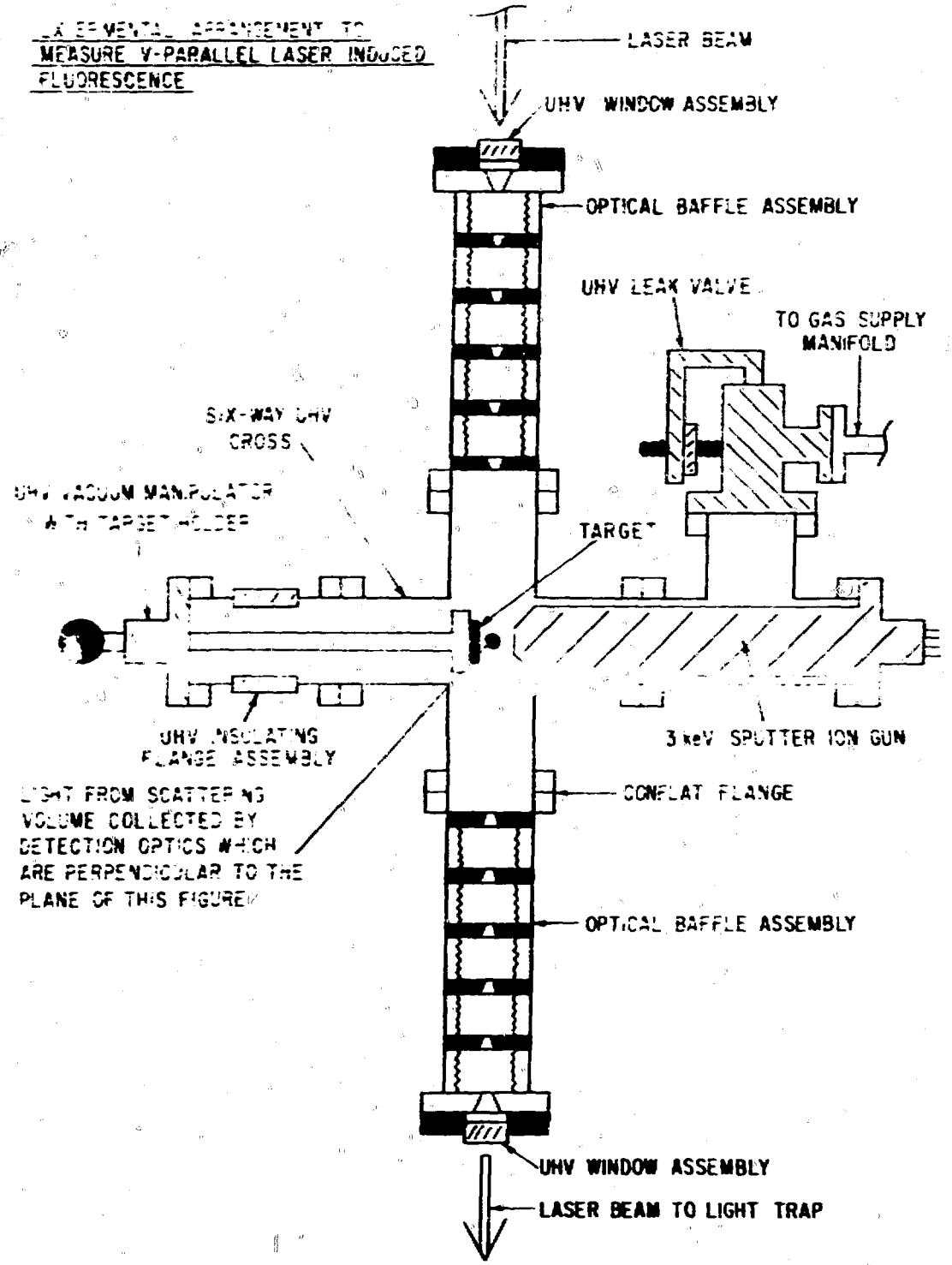

EXPERIMENTAL ARRANGEMENT TO MEASURE V-PARALLEL LASER INDUCED FLUORESCENCE

UHV VACUUM MANIPULATOR WITH TARGET HOLDER

LIGHT FROM SCATTERING VOLUME COLLECTED BY DETECTION OPTICS WHICH ARE PERPENDICULAR TO THE PLANE OF THIS FIGURE

Fig.2

EXPERIMENTAL ARRANGEMENT TO MEASURE V-PERPENDICULAR LASER INDUCED FLUORESCENCE

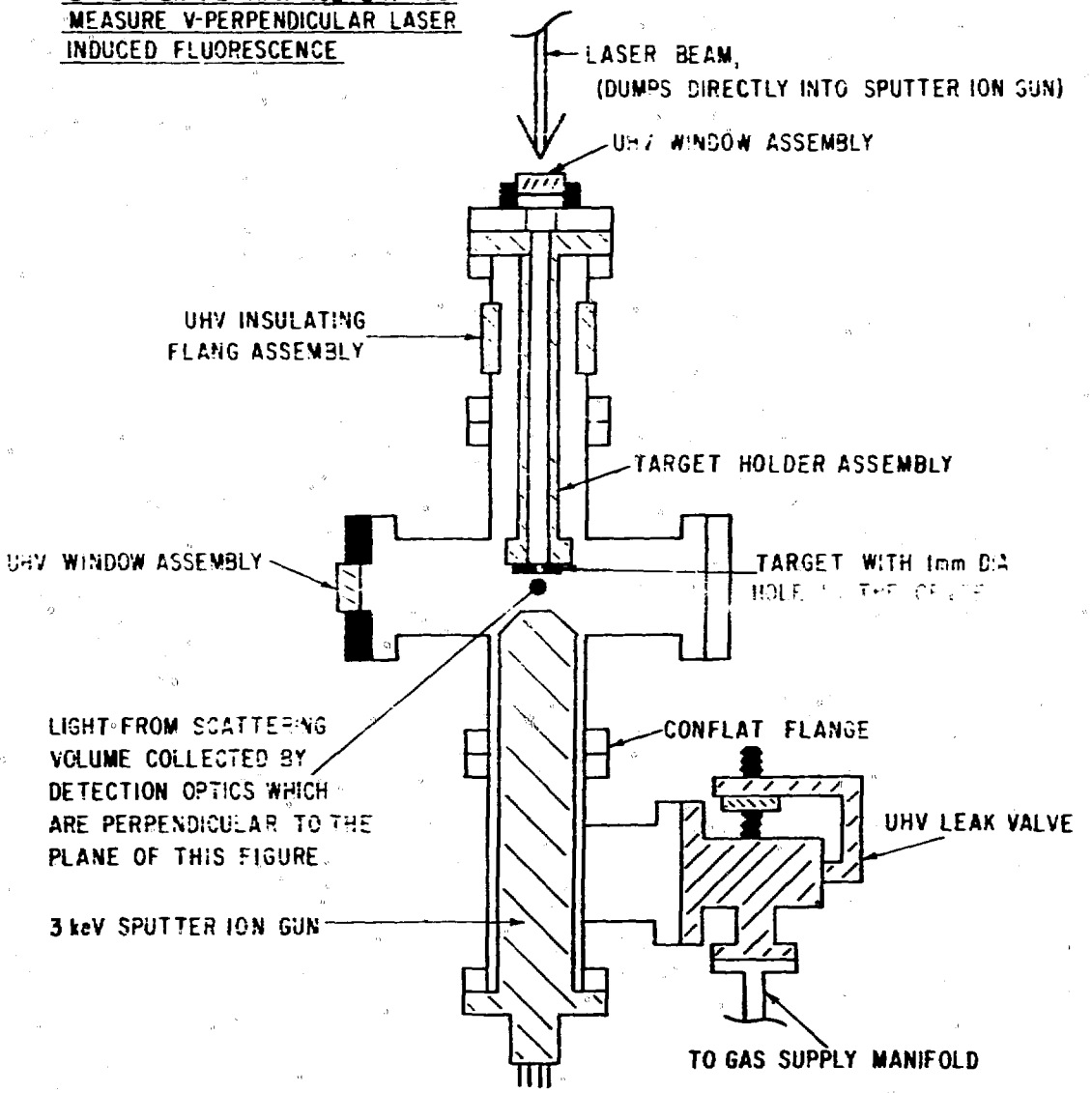

Fig. 3

PARTIAL ENERGY LEVEL DIAGRAM OF URANIUM (I)

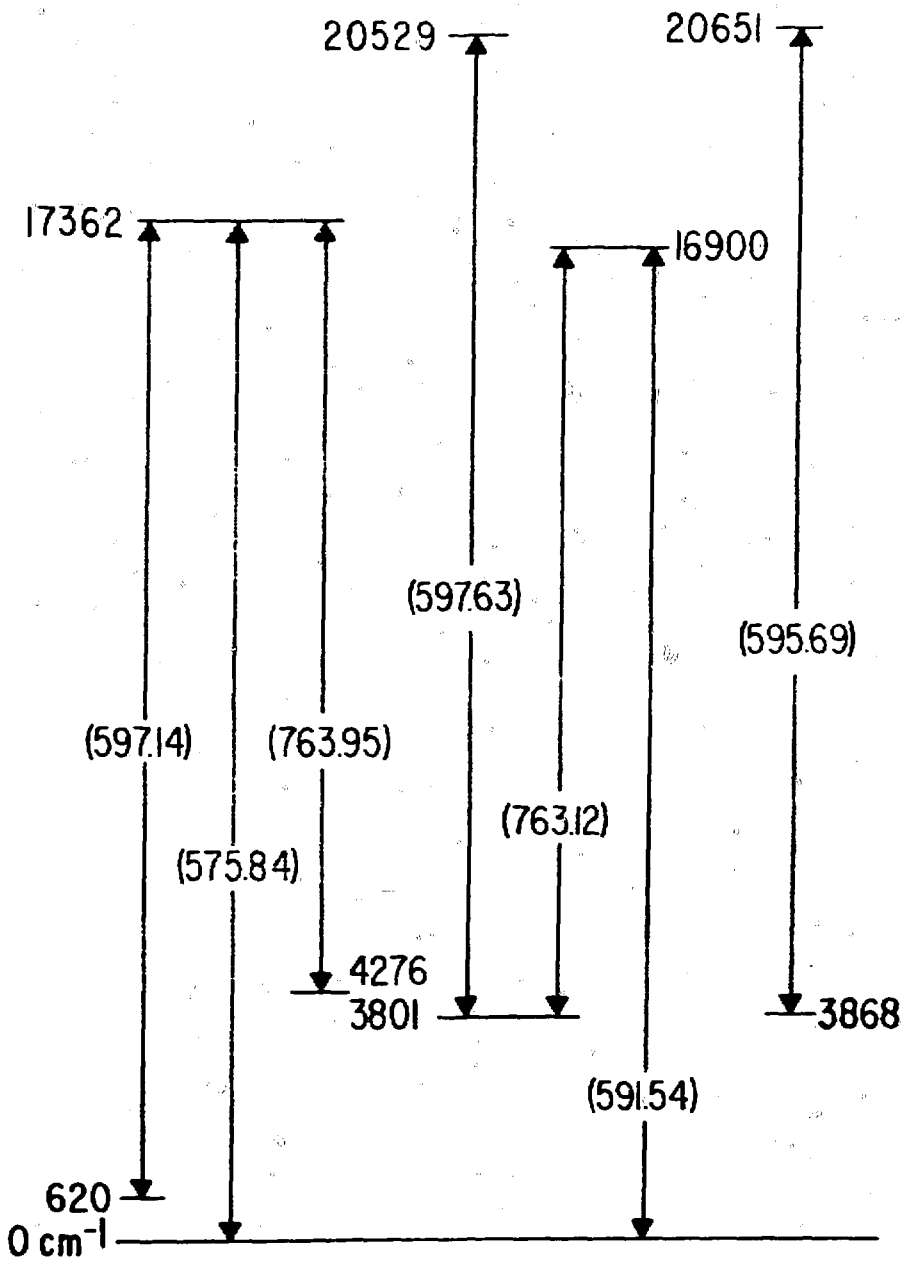

( ) VALUES ARE IN NANOMETERS FOR NORMAL AIR

cm^{-1} VALUES ARE IN VACUUM WAVE NUMBER UNITS

Fig. 4

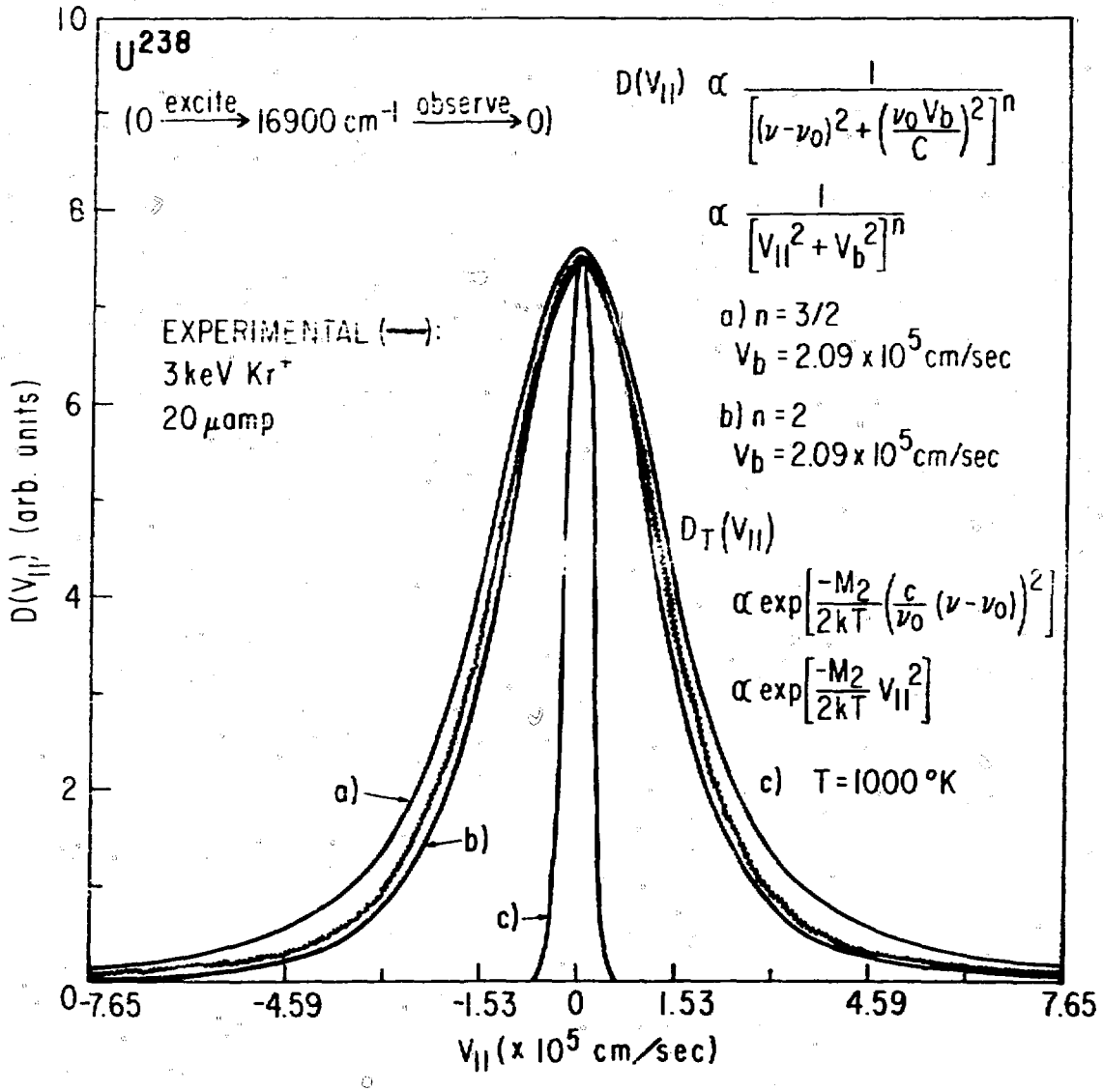
U238
(0 excite→ 16900 cm⁻¹ observe→ 0)
D(V_II) ∝ 1 / [(ν−ν0)² + (ν0 Vb / C)²]^n
∝ 1 / [V_II² + Vb²]^n
EXPERIMENTAL (—):
3 keV Kr⁺
20 μamp
a) n = 3/2
Vb = 2.09 x 10⁵ cm/sec
b) n = 2
Vb = 2.09 x 10⁵ cm/sec
D_T(V_II)
∝ exp[(-M2/2kT)(c/ν0 (ν−ν0))²]
∝ exp[(-M2/2kT) V_II²]
c) T = 1000 °K
D(V_II) (arb. units)
V_II (x 10⁵ cm/sec)
10
8
6
4
2
0
-7.65
-4.59
-1.53
0
1.53
4.59
7.65
a)
b)
c)

Fig. 5

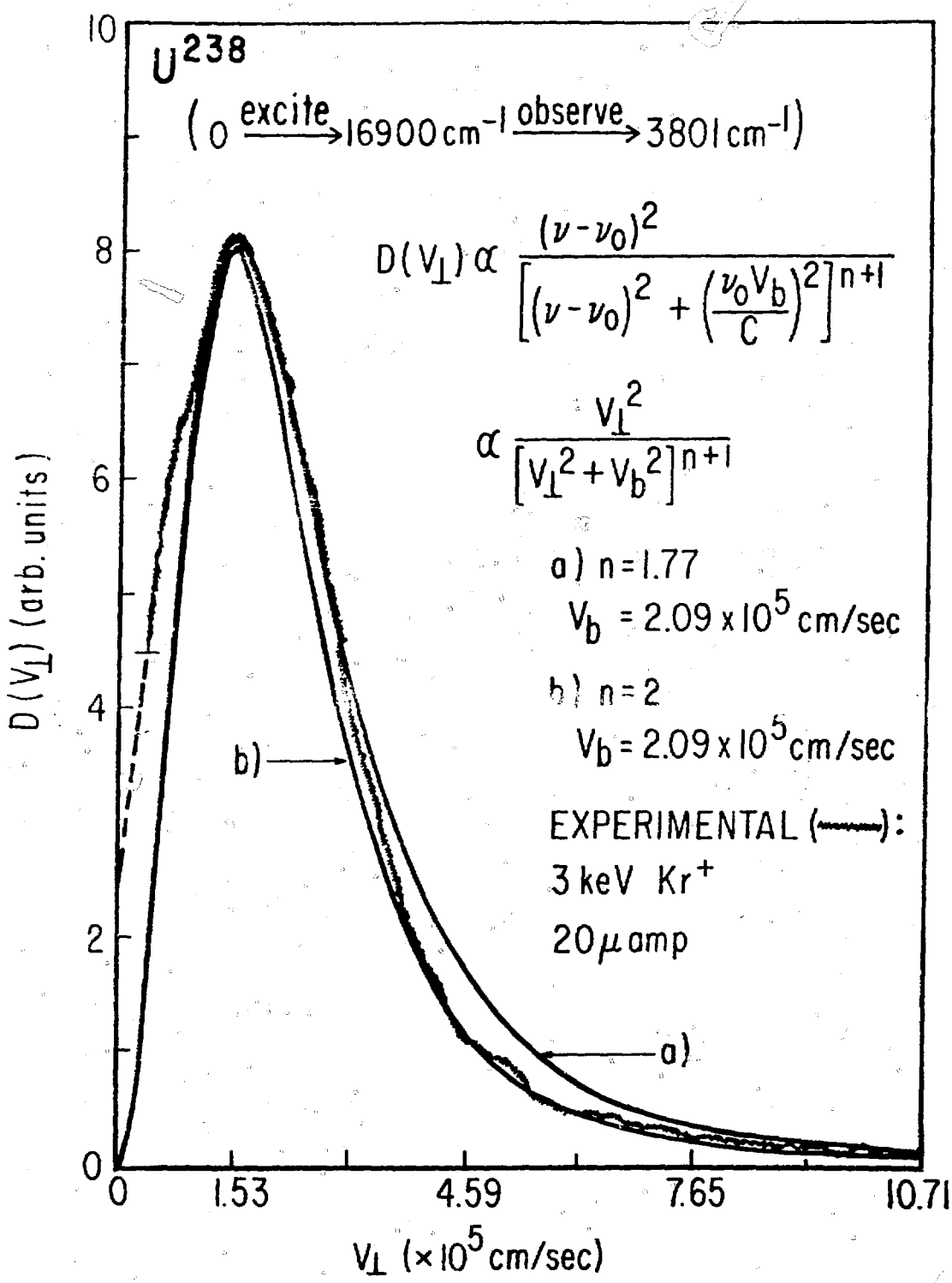
U238
(0 excite→16900 cm⁻¹ observe→3801 cm⁻¹)
D(V⊥) ∝ (ν − ν0)² / [(ν − ν0)² + (ν0 Vb / C)²]^(n+1)
∝ V⊥² / [V⊥² + Vb²]^(n+1)
a) n = 1.77
Vb = 2.09 x 10⁵ cm/sec
b) n = 2
Vb = 2.09 x 10⁵ cm/sec
EXPERIMENTAL (——):
3 keV Kr⁺
20 μamp
a)
b)
D(V⊥) (arb. units)
V⊥ (× 10⁵ cm/sec)
0
2
4
6
8
10
0
1.53
4.59
7.65
10.71

Fig. 6